Michigan State University

National Superconducting Cyclotron Laboratory

COMPARISON OF THE pnQRPA AND SHELL MODEL FOR GAMOW-TELLER AND DOUBLE-BETA DECAYS

LIANG ZHAO and B. ALEX BROWN

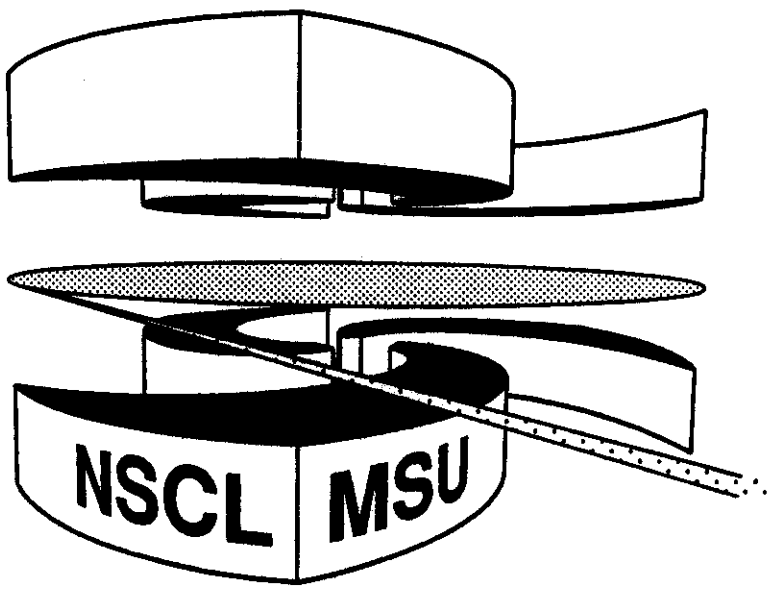

MSUCL-856

SEPTEMBER 1992

Comparison of the pnQRPA and Shell Model for Gamow-Teller Beta and Double-Beta Decays

Liang Zhao and B. Alex Brown

National *Superconducting Cyclotron Labomtoy*

and

Department of Physics and Astronomy, Michigan State University

East Lansing, MI 48824, USA

Abstract

We examine the validity of the pnQRPA as a model for calculating β^+ and $2\nu\beta\beta$ Gamow-Teller decays by making a comparison of the pnQRPA with a large-basis shell-model calculation within the $0f1p$ shell. Our comparison includes the decay matrix elements summed over final states, the strength distributions and coherent transition matrix elements (CTME). The CTME is introduced in order to study the single-particle state contributions to the total Gamow-Teller strength. The pnQRPA overestimates the total β^+ and $2\nu\beta\beta$ matrix elements. There are large differences in the shape of the spectra as well as in the CTME between the pnQRPA and shell-model results. Empirical improvements for the pnQRPA are discussed.

Contents

1 Introduction

The beta (β) decay process was one of the first types of radioactivity to be observed and still provides new valuable insight into weak interactions and nuclear structure [1, 2]. Nuclear double-beta ($\beta\beta$) decay phenomena is a rare transition between two nuclei of the same mass number having a change of two units of nuclear charge. In cases of interest, ordinary single beta decay is forbidden because of energy conservation or because of very strong suppression due to a large angular momentum mismatch between the parent and daughter states. There are two modes of double-beta decay [3, 4, 5, 6],

$$2\ \nu \text{ mode}: (A, Z) \rightarrow \quad (A, Z+2) + 2e^- + 2\bar{\nu}$$

$$0\ \nu \text{ mode}: (A, Z) \rightarrow \quad (A, Z+2) + 2e^-.$$

The first one is called two-neutrino (2ν) $\beta\beta$ decay, which involves the emission of two antineutrinos and two electrons (2ν mode), it occurs in second order in the standard weak interaction theory. Another is called neutrinoless (0ν) $\beta\beta$ decay, which involves the emission of two electrons and no neutrinos. This process violates the lepton number conservation and requires the neutrino to be a Majorana particle and have a nonzero mass and/or a nonstandard right-hand coupling [3, 4, 5, 6]. It occurs in some theories beyond the standard weak interaction model [3, 4, 5, 6]. The $2\nu\beta\beta$ decay has been observed in recent experiments [7, 8, 9, 10], but the $0\nu\beta\beta$ decay has not yet been observed.

There are two important nuclear models which have been applied to the study of β and $\beta\beta$ decays, the shell model and the proton-neutron Quasiparticle Random Phase Approximation (pnQRPA). Present shell-model theory, namely, the large-basis

shell model [11], assumes that the nuclear structure properties are determined by the valence nucleons which simultaneously occupy several different, partially filled, single-particle states. Thus the large-basis shell-model calculation takes into account many multi-nucleon configurations. Many experimental data for light nuclei (A$\leq$40) can be successfully explained and even predicted by the large-basis shell-model calculations [1, 11]. However, the dimension of the Hamiltonian matrix increases rapidly when the single-particle basis increases and the large-basis shell model becomes computationally impractical for most cases of interest with $A > 60$.

The pnQRPA was introduced by Halbeib and Sorensen [12] and further developed by Cha [13]. In this model, the excitations are constructed by acting two-quasiparticles creation and destruction operators on a ground state which is given by the BCS. The dimensions involved in the pnQRPA are relatively small so that it can be employed to study the β and $\beta\beta$ decays in all nuclei. In recent years, the pnQRPA has been used to calculate the Gamow-Teller transition strength in β and $\beta\beta$ in light and heavy nuclei [16, 17, 18, 19, 20, 21]. Several authors have investigated the particle-particle interaction term which was reintroduced by Cha [13], and found that the β^+ transition matrix elements and the $2\nu\beta\beta$ decay matrix elements are sensitive to this term [13, 16]. The total Gamow-Teller transitions strength and the $2\nu\beta\beta$ decay matrix elements are suppressed when the strength of the particle-particle interaction is increased [16, 22, 17, 18, 19, 20].

There may be some correlations that could be important in β^+ and $2\nu\beta\beta$ decay which are not included in the pnQRPA. Therefore it is very important to examine the validity and accuracy of the pnQRPA. These tests can be achieved by making a comparison of the pnQRPA and large-basis shell-model calculations in the nuclear mass regions where the large-basis shell-model calculations are possible. The large-

basis shell-model calculations include all types of correlations within a given set of single-particle states. Comparisons are most meaningful if the pnQRPA and shell-model calculations are performed in the same model space and use the same effective interaction.

This kind of comparison for β^+ decay has been made by Lauritzen [22] for several $1s0d$ shell nuclei, Brown and Zhao [23] for ^{28}Mg, Civitarese, et. al. [24] for ^{26}Mg and Auerbach, et. al. [25] for ^{26}Mg and ^{54}Fe. Lauritzen, Auerbach, Brown and Zhao concluded that the pnQRPA does not include some important correlations in β^+ decay and fails to reproduce the shell-model results. But Civitarese, et. al. appeared to contradict this conclusion.

In 1989, Brown and Zhao [23] made a comparison of the pnQRPA and large-basis shell-model calculations for hypothetical $\beta\beta$ decay of ^{28}Mg in the $1s0d$ shell. Later Muto et. al. [26] presented a similar comparison for the $\beta\beta$ decay of ^{48}Ca. But in their work, the model spaces of the pnQRPA and the shell model are not the same: the former is the $(1s0d + 0f1p0g)$ shells, and the latter is the $0f1p$ shell only. Therefore the comparison is confused because a meaningful comparison requires that the calculations of these models are performed in the same model space.

In this work, we will make a comparison of the pnQRPA and large-basis shell model within the $0f1p$ shell. Our comparison not only concentrates on the Gamow-Teller strength summed over all final states and/or their distributions, but also investigates the relative single-particle state contributions. The state-dependent gap equation in the BCS is used in our study. Some empirical improvements for the pnQRPA are discussed as well.

This paper is organized as follows. In section 2, the BCS and pnQRPA equations

are developed and the coherent transition matrix element (CTME), which describes the single-particle state contribution to the total strength, is introduced. Our comparison of the pnQRPA and shell model for β and $2\nu\beta\beta$ decays is presented in section 3.1 and 3.2, respectively. In section 4, a few possible improvements of the pnQRPA are discussed. In section 5, we give the summary and conclusions. In Appendix A and B, the QRPA and pnQRPA equations as well as their relationship are presented. In Appendix C, the coherent transition matrix element is discussed.

2 Formalism

2.1 pnQRPA equations

We start with the equation of motion [27, 28], where the excited eigenstates $|m>$ are constructed from the phonon creation operator $Q_m^\dagger$ which is defined by

$$|m>= Q_m^\dagger|0>, \text{ and } Q_m|0>= 0, \text{ for all } m \tag{1}$$

where $|m>$ and $|0>$ are the excited eigenstates and the physical ground state. They satisfy the Schrödinger equation,

$$H|m>= E_m|m> \text{ and } H|0>= E_0|0> . \tag{2}$$

Then one obtains the following equation of motion from the above relations;

$$[H, Q_m^\dagger]|0>= (E_m - E_0)Q_m^\dagger|0> . \tag{3}$$

Multiplying from the left with an arbitrary state of the form $<0|\delta Q_m$, we get

$$<0|[\delta Q_m, [H, Q_m^\dagger]]|0>= \hbar\omega <0|[\delta Q_m, Q_m^\dagger]|0> , \tag{4}$$

where $\hbar\omega = E_m - E_0$.

In order to obtain the pnQRPA equation, the phonon creation operators in the angular momentum coupled representation are written as [12, 13, 22],

$$Q^{\dagger}_{m}(J,M) = \sum_{p,n}(X^{\rm pn}_{m}\mathcal{A}^{\dagger}_{\rm pn}(pn,JM) - Y^{\rm pn}_{m}\tilde{\mathcal{A}}_{\rm pn}(pn,JM)), \quad (5)$$

$$\mathcal{A}^{\dagger}_{\rm pn}(pn,JM) = \sum_{m_p,m_n} < j_p m_p j_n m_n | JM > c^{\dagger}_{p,m_p} c^{\dagger}_{n,m_n}, \quad (6)$$

$$\tilde{\mathcal{A}}_{\rm pn}(pn,JM) = (-1)^{J+M}\mathcal{A}_{\rm pn}(pn,J-M), \quad (7)$$

where $c^{\dagger}_{j_{p(n)}}$ is the quasiproton (quasineutron) creation operator. The labels p/n stand for (nlj) for the proton/neutron single-particle states. In terms of the spherical shell-model states, the particle and quasiparticle creation and destruction operators are related by the Bogoliubov transformation, e.g. for proton

$$c^{+}_{p,m_p} = u_p a^{+}_{p,m_p} + (-)^{j_p+m_p} v_p a_{p,-m_p}, \quad (8)$$

where $u_p^2 + v_p^2 = 1$, and $a^{\dagger}_{p}$ is the proton creation (destruction) operator for the single-particle state. v_p^2 turns out to be the proton occupation probability. The eigenvalue $\hbar\omega$ and the forward- and backward- going amplitudes X and Y are obtained by solving the pnQRPA equation

$$\begin{pmatrix} A & B \\ -B^{*} & -A^{*} \end{pmatrix}\begin{pmatrix} X \\ Y \end{pmatrix} = \hbar\omega \begin{pmatrix} X \\ Y \end{pmatrix}, \quad (9)$$

with the orthogonality relation

$$\sum_{pn}[X^{pn}_{m}X^{pn}_{m'} - Y^{pn}_{m}Y^{pn}_{m'}] = \delta_{mm'}. \quad (10)$$

The matrix elements A and B are explicitly given by [12, 13, 22, 16]

$$A^{J}_{pnp'n'} = < \mathrm{QRPA}|[\mathcal{A}_{\rm pn}(pn,JM),[H,\mathcal{A}^{\dagger}_{\rm pn}(p'n',JM)]]|\mathrm{QRPA} >$$
$$\simeq < \mathrm{BCS}|[\mathcal{A}_{\rm pn}(pn,JM),[H,\mathcal{A}^{\dagger}_{\rm pn}(p'n',JM)]]|\mathrm{BCS} >$$

$$= (E_p + E_n)\delta_{pp'}\delta_{nn'} + (H_{22}^{\rm pn})^J_{pnp'n'}, \tag{11}$$

$$B^J_{pnp'n'} = < \mathrm{QRPA}|[\mathcal{A}_{\rm pn}(pn, JM), [H, \tilde{\mathcal{A}}_{\rm pn}(p'n', JM)]]|\mathrm{QRPA} >$$

$$\simeq < \mathrm{BCS}|[\mathcal{A}_{\rm pn}(pn, JM), [H, \tilde{\mathcal{A}}_{\rm pn}(p'n', JM)]]|\mathrm{BCS} >$$

$$= -(G^{\rm pn})^J_{pnp'n'}, \tag{12}$$

with

$$(H_{22}^{\rm pn})^J_{pnp'n'} = g_{pp}V^J_{pnp'n'}(u_pu_nu_{p'}u_{n'} + v_pv_nv_{p'}v_{n'})$$

$$+g_{ph}W^J_{pnp'n'}(u_pv_nu_{p'}v_{n'} + v_pu_nv_{p'}u_{n'}), \tag{13}$$

$$(G^{\rm pn})^J_{pnp'n'} = g_{pp}V^J_{pnp'n'}(u_pu_nv_{p'}v_{n'} + v_pv_nu_{p'}u_{n'})$$

$$-g_{ph}W^J_{pnp'n'}(v_pu_nu_{p'}v_{n'} + u_pv_nv_{p'}u_{n'}). \tag{14}$$

where $|\mathrm{QRPA}>$ is the QRPA ground state defined in Appendix A. The relation between the QRPA and pnQRPA is discussed in Appendix B. The quasiproton and quasineutron energies E_p and E_n and occupation factors u, v are obtained by solving the BCS equation in section 2.2. The matrix elements of the particle-particle (V) and particle-hole (W) interaction are related by Pandya transformation,

$$W^J_{pn,p'n'} = -(-1)^{j_p+j_n+j_{p'}+j_{n'}}\sum_{J'}(2J'+1)\left\{\begin{array}{ccc} j_p & j_n & J \\ j'_p & j'_n & J' \end{array}\right\}V^{J'}_{pn',p'n}. \tag{15}$$

In order to discuss the results as a function of the strength associated with each part of the interaction, the multiplicative factors g_{ph} and g_{pp} are conventionally introduced for the particle-particle and particle-hole, respectively. They are both equal to unity in the standard pnQRPA theory.

The charge-exchange transition matrix elements of the Gamow-Teller operator between the ground state $|0^+_i>$ and the excited state $|1^+_m>$ are given by

$$B(\mathrm{GT}) = \frac{1}{2J_i+1}(< J^\pi_m||\sigma t||J^\pi_i >)^2, \tag{16}$$

where $J_m^\pi = 1_m^+$ and $J_i^\pi = 0_i^+$ in our example. We denote

$$M_m(\mathrm{GT}) = < J_m^\pi || \sigma t || J_i^\pi > , \tag{17}$$

where σ is the Pauli spin operator. The isospin operator t can be the raising or lowering operator, t^+ or t^-, corresponding to β^+ and β^- Gamow-Teller transitions, respectively. In the pnQRPA, one obtains

$$M_m(\mathrm{GT}^-) = \sum_{pn} < p||\sigma||n > (X_m^{pn} u_p v_n + Y_m^{pn} v_p u_n), \tag{18}$$

$$M_m(\mathrm{GT}^+) = -\sum_{pn} < p||\sigma||n > (X_m^{pn} v_p u_n + Y_m^{pn} u_p v_n). \tag{19}$$

The above equations for $M_m(\mathrm{GT})$ in the pnQRPA can be rewritten as,

$$M_m(\mathrm{GT}) = \sum_{pn} < p||\sigma||n > \mathrm{OBTD}(p,n,m,i)_{\mathrm{QRPA}}, \tag{20}$$

where the $\mathrm{OBTD}(p,n,m,i)_{\mathrm{QRPA}}$ is a one-body transition density. The Gamow-Teller matrix elements summed over all final states, J_m^π, satisfy the sum rule,

$$\sum B(\mathrm{GT}^-) - \sum B(\mathrm{GT}^+) = 3(N-Z). \tag{21}$$

2.2 BCS equations

In the BCS approximation, the quasiproton energies E_p, occupation probabilities v_p^2 and pairing gaps Δ_p are given by [33]

$$E_p = \sqrt{(\varepsilon_p - \lambda_\pi)^2 + \Delta_p^2}, \tag{22}$$

$$v_p^2 = \frac{1}{2}\left(1 - \frac{\varepsilon_p - \lambda_\pi}{\sqrt{(\varepsilon_p - \lambda_\pi)^2 + \Delta_p^2}}\right), \tag{23}$$

$$\Delta_p = -\sum_{p'} \sqrt{\frac{2j'_p + 1}{2j_p + 1}} u_{p'} v_{p'} V_{pp,p'p'}^{J=0}, \tag{24}$$

where λ_π is the proton Fermi energy, ε_p is the single proton energy and $V_{pp,p'p'}$ is the proton two-body interaction. The above equations are solved with the constraint for the total proton number

$$N_\pi = \sum_p (2j_p + 1)v_p^2, \tag{25}$$

to determine the constant λ_π. A similar set of the equations is solved for neutrons. The single proton energies ε_p are related to the bare single-particle proton energies ε_p^0 at the closed shell by addition of the rearrangement terms Γ_p

$$\varepsilon_p = \varepsilon_p^0 + \Gamma_p, \tag{26}$$

where

$$\begin{aligned} \Gamma_p &= \frac{1}{2j_p+1}\sum_{p'}(1+\delta_{pp'})v_{p'}^2 \sum_J (2J+1)V^J_{pp',pp'} \\ &+ \frac{1}{(2j_p+1)}\sum_{n'} v_{n'}^2 \sum_J (2J+1)V^J_{pn',pn'}. \end{aligned} \tag{27}$$

The first term refers to like particle correction and the second term to unlike particle correction. The rearrangement term for ε_n has the same form but with the p/n indices interchange. The BCS equations (22-25) plus the rearrangement terms can be solved iteratively.

We note that the input ingredients in the BCS (Eqs. (9 – 14)) and the pnQRPA (Eqs. (22 – 27)), in our formalism, are consistent with those in the shell model, namely, the bare single particle energies ε_j^0 at the closed shell and two-body interaction matrix elements V^J_{ijkl}. The Coulomb shift is taken into account in both shell model and pnQRPA in our comparison [32].

2.3 B(GT) in shell-model calculations

In the shell-model calculation, the Gamow-Teller strength is equal to the product of one-body transition density and single particle matrix element [1], and the matrix element M_m in Eq. (17) is expressed by

$$M_m(\mathrm{GT}) = \sum_{pn} < p||\sigma||n > \mathrm{OBTD}(p,n,m,i)_{\mathrm{SM}}, \tag{28}$$

where

$$\mathrm{OBTD}(p,n,m,i)_{\mathrm{SM}} =< J_m^\pi||\frac{[a_p^+ \otimes \tilde{a}_n]^{\Delta J}}{\sqrt{2\Delta J+1}}||J_i^\pi > , \tag{29}$$

The shell model wave function $|J_m^\pi >$ and $|J_i^\pi >$ as well as $\mathrm{OBTD}(p,n,m,i)_{\mathrm{SM}}$ are calculated with the OXBASH shell-model code [29]. The proton (neutron) occupation probabilities in the shell model are given by

$$v^2_{p(n)}(\mathrm{SM}) = \frac{< J_i^\pi|a^+_{p(n)}a_{p(n)}|J_i^\pi >}{2j_{p(n)}+1}, \tag{30}$$

For the Gamow-Teller transitions in our example, we have $|J_m^\pi >= |1_m^+ >$, $|J_i^\pi >= |0_i^+ >$ and $\Delta J = 1$.

2.4 The coherent transition matrix elements

The B(GT) spectrum itself lacks information about the single-particle state contributions in the charge-exchange process, because we sum over all single-particle state components p,n in Eqs.(18–20) for the pnQRPA and Eq.(28) for the shell model. Therefore, we introduce new quantities which can describe such single-particle state contributions to the total strength. We define the *coherent one-body transition density* (COBTD) as

$$\mathrm{COBTD}(p,n,i) = \frac{1}{\sqrt{\sum_m B(\mathrm{GT})}} \sum_m M_m(\mathrm{GT})\mathrm{OBTD}(p,n,m,i), \tag{31}$$

where $M_m(\mathrm{GT})$ is given by Eq. (17). The OBTD is given by Eq. (29) and (20) for the shell model and the pnQRPA, respectively. Also the *coherent transition matrix element* (CTME) is defined by

$$\mathrm{CTME}(p,n,i) =< p||\sigma||n > \mathrm{COBTD}(p,n,i). \tag{32}$$

The COBTD and CTME are a function of the single-particle state components. All final states(m) are summed up in Eq. (31). The relation between the total $B(\mathrm{GT})$ and the CTME is given by

$$\{\sum_{p,n} \mathrm{CTME}(p,n,i)\}^2 = \sum_m B(\mathrm{GT}). \tag{33}$$

In Appendix C, we will discuss the derivation of the CTME.

2.5 Formalism of $2\nu\beta\beta$ decay

In the shell-model calculations, the (intermediate state) energy dependent matrix element is defined by

$$M_{\mathrm{GT}}(E_m) = \sum_{m=1}^{E_m} \frac{< J_f^\pi||\sigma t^-||J_m^\pi >< J_m^\pi||\sigma t^-||J_i^\pi >}{E_m - E_i + T_0/2 + m_e c^2}, \tag{34}$$

where E_m are the excitation energies of the intermediate states, E_i is the intial state energy, $T_0/2$ is the Q-value of $\beta\beta$ decay, and $m_e c^2$ is electron mass. The total matrix element for $2\nu\beta\beta$ is given by $M_{\mathrm{GT}} = M_{\mathrm{GT}}(E_m = \infty)$. The closure matrix element is defined by

$$B_{\mathrm{CLS}}(E_m) = \sum_{m=1}^{E_m} < J_f^\pi||\sigma t^-||J_m^\pi >< J_m^\pi||\sigma t^-||J_i^\pi > . \tag{35}$$

The total matrix element is given by $B_{\mathrm{CLS}} = B_{\mathrm{CLS}}(E_m = \infty)$. In our example, $J_i^\pi = 0_i^+$, $J_f^\pi = 0_f^+$ and $J_m^\pi = 1_m^+$.

In the pnQRPA calculations, the $\beta\beta$ formulas become more complicated because the summation in Eqs. (34 – 35) involves the product of two transition matrix

elements and each one contains the intermediate states of the intermediate nucleus. Of course, in the shell model, the intermediate states in the two transition matrix elements are the same. But in the pnQRPA, we recognize that the intermediate states in the two transition matrix elements are different. They depend on which parent nucleus is being considered. Thus a problem arises that the intermediate states resulting from the two different pnQRPA calculations are not orthogonal. Of course, they should be the same physically. In order to solve such a mismatch problem, one can introduce an overlap matrix element between any two intermediate states J^π_m and $J^\pi_{m'}$, [18, 20],

$$< J^\pi_m | J^\pi_{m'} >= \sum_{pn} (\bar{X}^{pn,J^\pi}_{m'} X^{pn,J^\pi}_m - \bar{Y}^{pn,J^\pi}_{m'} Y^{pn,J^\pi}_m) \tag{36}$$

where m, m' denote two states with eigenvectors (X, Y) and $(\bar{X}, \bar{Y})$, which are constructed from intial and final states, respectively [18, 30, 20]. Obviously, if (X, Y) and $(\bar{X}, \bar{Y})$ are identical, then we have $< J^\pi_m | J^\pi_{m'} >= \delta_{mm'}$ (see Eq. (10)). With the overlap matrix element, Eq. (34 - 36) can be rewritten as

$$M_{\rm GT}(E_m) = \sum_{m,m'} \frac{< 0^+_f || \sigma t^- || 1^+_m >< 1^+_m | 1^+_{m'} >< 1^+_{m'} || \sigma t^- || 0^+_i >}{E_m - E_i + T_0/2 + m_e c^2}, \tag{37}$$

$$B_{\rm CLS}(E_m) = \sum_{m,m'} < 0^+_f || \sigma t^- || 1^+_m >< 1^+_m | 1^+_{m'} >< 1^+_{m'} || \sigma t^- || 0^+_i > . \tag{38}$$

3 Comparison of the pnQRPA and shell model

3.1 Comparison for β decay

In this subsection, we compare the results between the pnQRPA and large-basis shell model for β^+-decay of ^{46}Ti and β^--decay of ^{46}Ca. The model space is the full $0f1p$ shell and the effective interaction used is MSOBEP [31].

In the BCS equations given by section 2.2, the pairing gaps and single-particle rearrangement terms are state dependent and are self-consistently calculated. In Table 1 and 2, the BCS single-particle energies with the addition of rearrangement terms, quasiparticle energies, pairing gaps and occupation probabilities of ^{46}Ti and ^{46}Ca are presented. The proton pairing gaps are about 40 % less than those obtained from the empirical formula $\Delta_p = 12A^{-1/2}$.

We define the running sum as

$$B(\mathrm{GT}^+, E_m) = \sum_{m=1}^{E_m} (< 1_m^+ || \sigma t^+ || 0_i^+ >)^2, \tag{39}$$

$$B(\mathrm{GT}^-, E_m) = \sum_{m=1}^{E_m} (< 1_m^+ || \sigma t^- || 0_i^+ >)^2. \tag{40}$$

The total $B(\mathrm{GT}^+)$ and total $B(\mathrm{GT}^-)$ are given by $E_m = \infty$.

Figure 1 and 2 present the $B(\mathrm{GT}^+, E_m)$ and $B(\mathrm{GT}^-, E_m)$ as a function of the ^{46}Sc 1^+ excitation energy E_m corresponding to ^{46}Ti and ^{46}Ca ground state, respectively. The pnQRPA and shell-model results are shown by dashed and solid lines, respectively.

The J-dimensions in our large-basis shell-model calculations are 24, 1514 and 2042 for the ^{46}Ca ground state, the ^{46}Sc 1^+ excitations and the ^{46}Ti ground state, respectively.

Figure 1 shows three major differences between the results of the pnQRPA and the shell model in the β^+ Gamow-Teller strength: (i) the pnQRPA calculation does not give sufficient suppression for the total $B(\mathrm{GT}^+)$; (ii) the energies of the first excited state in the two models differ by about 6 MeV. (iii) the strength distributions in two models are mismatched. The shell-model Gamow-Teller strength is mainly concentrated at its low-excitation energy, but in the pnQRPA, the strength distribution is

much broader.

The coherent transition matrix elements (CTME) defined by section 2.4 are given in Table 3 for the pnQRPA and shell model, (see columns (A) and (E)). There are significant differences between the two models. Most importantly, the CTME values in the pnQRPA and shell model have the opposite sign for the $f_{7/2} \rightarrow f_{7/2}$.

For ^{46}Ca, there is no valence proton in the $0f1p$ shell (i.e., $v_p = 0$), so the matrix B in the pnQRPA is zero and the pnQRPA reduces to the pnQTDA, where the amplitudes Y are equal to zero. In this case, the β^+ transition strength of ^{46}Ca vanishes and the total $B(\mathrm{GT}^-)$ strength is equal to 18 because of the sum rule Eq. (21). In Figure 2, the first 1^+ eigenvalue of the pnQRPA differs by about 5 MeV from that of the shell model.

3.2 Comparison for $2\nu\beta\beta$ decay

In this subsection, we compare the results of the pnQRPA and large-basis shell model for the $2\nu\beta\beta$ of ^{46}Ca. In this case, the initial (final) nucleus has 0 (2) protons and 6 (4) neutrons in the $0f1p$ shell. The double-beta decay matrix elements M_{GT} and/or B_{CLS} consist of the virtual decay routes, β^- and β^+ decays. Their Gamow-Teller strengths in the pnQRPA and shell model were presented and discussed in the last section.

In Figure 3 and 4, we present the running sum of matrix element $B_{\mathrm{CLS}}(E_m)$ and $M_{\mathrm{GT}}(E_m)$ as a function of the 1^+ excitation energies corresponding to the ^{46}Ca ground state. The excitation energies are obtained from the pnQRPA calculation for ^{46}Ca $\rightarrow ^{46}$Sc, and are employed to evaluate the energy denominator in Eq. (37), but the first 1^+ state in the pnQRPA is shifted to the position of the first 1^+ state in the

shell model in order to use a consistent energy denominator to calculate $M_{\rm GT}(E_m)$. In practice, the first 1^+ state in the $2\nu\beta\beta$ calculation is chosen by using the experimental value [35, 36]. (In our case, the shell model and experiment are essentially the same for the position of the lowest 1^+ state energy.)

Qualitatively the pnQRPA and shell-model show a similar shape. There is a cancellation between the matrix elements in the low- and high-lying states. The magnitudes, however, are very different. We find the pnQRPA does not provide enough suppression for total $M_{\rm GT}$ and $B_{\rm CLS}$, which are about three to four times larger than those in the large-basis shell-model calculation. The largest difference in the matrix elements are shown in the low-lying states between the two models. For example, the first $M_{\rm GT}(E_1)$ and $B_{\rm CLS}(E_1)$ are almost 5 times larger than the corresponding shell-model results. In the pnQRPA, the first $B({\rm GT}^-)$ and $B({\rm GT}^+)$ are dominated by the transition $f_{7/2} \rightarrow f_{7/2}$, but in the shell model, this transition contributes only about 50 %.

Finally, in Eqs. (37,38), we can also calculate the $2\nu\beta\beta$ decay matrix elements by projecting the 1^+ excitations from ^{46}Ca β^- decay onto ones from ^{46}Ti β^+ decay and using the corresponding energy denominators. The results are similar to those discussed above.

3.3 Sensitivity to the particle-particle interaction

Since the $B({\rm GT}^+)$ strength and $2\nu\beta\beta$ decay matrix elements $B_{\rm CLS}$ and $M_{\rm GT}$ are more sensitive to g_{pp} than to g_{ph}, we will set $g_{ph} = 1$ and discuss the dependence on g_{pp}. In Figure 5, the $B({\rm GT}^+)$ spectra with various g_{pp} values are presented. We find the pnQRPA results are very sensitive to g_{pp}, in agreement with the previous conclusions [13, 22, 16]. The total shell-model $B({\rm GT}^+)$ is reproduced by the pnQRPA

with $g_{pp} = 1.4$, but the shape of the strength distributions of two models are totally different.

When g_{pp} increases beyond a certain value, the lowest eigenvalue becomes the imaginary and the pnQRPA equation collapses. It means that the pnQRPA theory is no longer a valid model. Around this g_{pp}, the equation gives unrealistic large amplitudes X and Y.

In Figure 6 and 7, we present $M_{\rm GT}(E_m)$ and $B_{\rm CLS}(E_m)$ with respect to various g_{pp} values. The particle-particle interaction suppresses the total matrix elements in agreement with previous studies [17, 18, 19, 20]. If the particle-particle channel is shut off ($g_{pp} = 0$), the cancellation of $B_{\rm CLS}(E_m)$ between the low- and high-lying excitations disappears. However, the cancellation emerges and becomes stronger as g_{pp} is increased.

4 Phenomenological improvements of pnQRPA

We now investigate various ways to understand and then improve the agreement between the pnQRPA and the large-basis shell model.

As we alluded in last section, the $B(\mathrm{GT}^+)$ strength in the pnQRPA is spread out compared with the shell-model result. This is partly related to the fact that the 1^+_m excitations constructed from the ^{46}Ti ground state in the pnQRPA do not have good isospin. The ^{46}Ti ground state has isospin $T = 1$. The β^- Gamow-Teller decay can go to the excitations with T =0, 1 and 2. The β^+ Gamow-Teller decay only go to the excitations with T =2. In the shell model, the excited states with various T are, of course, independent. However, in the pnQRPA, the energy spectra of the 1^+_m states in both β^- and β^+ are exactly the same. The β^- and β^+ Gamow-Teller strengths are

different due to the various combination of the X and Y amplitudes (Eqs. (18.19). The consequence of this is that the lowest 1^+_m state in β^+ which should be pure $T = 2$ is (due to the spurious isospin mixing) mainly from the $T = 0$ 1^+_m state and hence is much to low in energy. But the $1^+_{m'}$ states constructed from the ^{46}Ca ground state have much better isospin because the β^+ Gamow-Teller decay is forbidden in the $0f1p$ shell. Thus we project the 1^+_m states obtained in the ^{46}Ti β^+ calculation onto the $1^+_{m'}$ states obtained in the ^{46}Ca β^- calculation and re-define the $M_m(\mathrm{GT}^+)$ in Eq.(17) as

$$M_m(\mathrm{GT}^+) = \sum_{m'} < J^\pi_{m'} || \sigma t^+ || J^\pi_i > < J^\pi_{m'} | J^\pi_m > , \qquad (41)$$

where the projection factor $< J^\pi_{m'} | J^\pi_m >$ is given by Eq. (36). The running sum $B(\mathrm{GT}, E_m)$ for the re-defined $M_m(\mathrm{GT}^+)$ is shown in Figure 8. We find that the shape of of the $B(\mathrm{GT}^+)$ strength distribution is now in much better agreement with the shell model. The CTME given in Table 3 do not change significantly.

Another empirical improvement might be achieved by using some shell-model quasiparticle energies and/or occupation probabilities in the pnQRPA. These types of the modified models are called " hybrid " pnQRPA.

Now we introduce the shell-model quasiparticle energies. Since the BCS quasiparticle energies can be understood as the lowest excited energies of the odd nucleus [27, 33], one may appropriately analyse the odd nucleus energy spectra in the shell-model calculations, and find those excited states which are qualitatively equivalent to the single quasiparticle E_j excitations. For example, the shell-model quasineutron energies of ^{46}Ti can be obtained as follows: the one-particle transfer amplitudes are calculated between the ^{46}Ti ground state and the ^{47}Ti excited states $J = 7/2^-$ (or $3/2^-$, $5/2^-$ and $1/2^-$). The eigenvalue of the state which has the largest overlap in one-particle transfer is considered as the shell-model quasineutron energy $E_{f_{7/2}}$ (or

$E_{p_{3/2}}$, $E_{f_{5/2}}$ and $E_{p_{1/2}}$). The shell-model occupation probabilities are defined by Eq. (30). The shell-model occupation probabilities and quasiparticle energies for proton and neutron of ^{46}Ti are given in the Table 1 and compared with the BCS results.

The calculations for three types of " hybrid " pnQRPA are shown in Figure 9. The dashed line is the pnQRPA with BCS occupations and shell-model quasiparticle energies. The dotted line is the pnQRPA with shell-model occupations and BCS quasiparticle energies. The dot-dashed line is the pnQRPA with shell-model occupations and quasiparticle energies. One finds that the total $B(\mathrm{GT}^+)$ strength is suppressed in the " hybrid " pnQRPA. That is 2.187 in the pnQRPA, 1.959 in the " hybrid " pnQRPA with the shell-model quasiparticle energies and the BCS occupation probabilities, 1.687 in the " hybrid " pnQRPA with the BCS quasiparticle energies and the shell-model occupation probabilities, and 1.335 in the " hybrid " pnQRPA with the shell-model quasiparticle energies and the occupation probabilities. The latter is close to 0.928 obtained for the total $B(\mathrm{GT}^+)$ in the large-basis shell model.

The " hybrid " models have not improved the strength distribution. But comparing to the shape of the spectrum of the pnQRPA with $g_{pp} = 1.4$ in Figure 1, the " hybrid " pnQRPA with the shell-model parameters (the dot-dashed line in Figure 9) still keeps a reasonable shape. In the " hybrid" pnQRPA, the position of the 1^+ state almost remains the same, i.e., it still differs by 6 MeV from the shell-model calculation.

The CTME values of the " hybrid " pnQRPA are presented in the columns (B), (C)and (D) of Table 3. The CTME in the column (B) are obtained by using the shell-model quasiparticle energies and the BCS occupation probabilities in the pnQRPA.

We find that the difference between the columns (B) and (E) is decreased only for the transitions $f_{7/2} \rightarrow f_{7/2}$, but the CTME in other transitions become worse or remain the same. The CTME values in column (C), using the BCS quasiparticle energies and the shell-model occupation probabilities, and column (D), using the shell-model quasiparticle energies and the occupation probabilities, present a similar behaviour. The CTME in the transition $f_{7/2} \rightarrow f_{7/2}$ now have the same sign as those in column (E). The CTME for the transition $p_{3/2} \rightarrow p_{1/2}$ are and $f_{5/2} \rightarrow f_{5/2}$ have been improved over those in the pnQRPA. But other CTME values become worse compared to those in the pnQRPA.

We compare the occupation factors between the BCS and shell-model in Table 1 and find in order to reproduce shell-model occupation factors, the pairing gap in the BCS equation should be unrealistically increased to around 4 Mev [22]. It requires a very strong and unrealistical effective interaction. The present BCS gaps are around 1 MeV.

Encouraged by the successes of the improvements of the pnQRPA we also consider the use of " hybrid " models for the $\beta\beta$ decay matrix elements. The shell-model quasiparticle energies and occupation probabilities for the initial and final nuclei are given in Table 1 and Table 2. In Figure 10, the solid line is from the shell model, the dashed line is from using the shell-model quasiparticle energies in the pnQRPA, the dotted line from using the shell-model occupation numbers, and dash-dotted line from using shell model quasiparticle and occupation probabilities. We find that the "hybrid" pnQRPA can not give enough suppression for total $B_{\rm CLS}$ to reproduce the shell-model results. One may conclude the " hybrid " models do not work well for $2\nu\beta\beta$ decay.

5 Summary and conclusions

The nuclear shell model and the pnQRPA equation are very important nuclear structure theories for studying β and $\beta\beta$ decays. But the approach of these two models is different. Many or all types of many-body correlations are taken into account in the large-basis shell-model calculations. The pnQRPA is an approximate model, which includes only some special classes of the correlations. The goal of this paper was to examine the validity and accuracy of the pnQRPA for β^+ and $\beta\beta$ processes. The examination is achieved by making a comparison of the pnQRPA and the large-basis shell-model calculations in the $0f1p$ shell.

In section 2, the BCS and pnQRPA have been developed. The input ingredients in the BCS and pnQRPA are the same as those in the shell model, namely, the bare single particle energies at the closed shell and two-body interaction matrix elements. Therefore there is no free parameter for both models in our comparison. The coherent transition matrix elements (CTME) are introduced for analysis of the single-particle state contributions in β decay. In section 3, we have investigated the accuracy of the pnQRPA approach to β and $\beta\beta$ decays. Comparisons of the pnQRPA and large-basis shell-model calculations have been made. Our comparisons have shown the pnQRPA overestimates the total $B(\mathrm{GT}^+)$ and $\beta\beta$ decay matrix elements, and there are large discrepancies in the shapes of the strength distributions between the pnQRPA and shell-model calculations. The CTME of the pnQRPA are also in poor agreement with those of the shell-model. Thus we may conclude there must be some correlations which are important to β and $2\nu\beta\beta$ decay but have not been included in the pnQRPA.

Two types of empirical improvement for the pnQRPA were suggested in section 4. One was to project the β^+ energy spectra onto the β^- spectra in order to have

relatively good isospin. The shape of the strength distribution after projection is close to the shell-model result. Another was the " hybrid " pnQRPA, which was obtained by using the shell-model occupation probabilities and the shell-model quasiparticle energies in the pnQRPA. About 50 % suppressions are found for the total $B(\mathrm{GT}^+)$ strength. The shape of the $B(\mathrm{GT}^+)$ distribution has not been improved but it is more reasonable than that in the pnQRPA with larger g_{pp} values. But for $2\nu\beta\beta$ decay, we find the " hybrid " pnQRPA does not work very well. The Gamow-Teller β^+ strength and double-beta decay matrix element in medium and heavy nuclei will continue to be a challenge for nuclear structure models.

Acknowledgements: We would like to thank Dr. A. Sustich and Dr. D. Cha for their helpful discussions. This work was supported by the National Science Foundation under Grants No. PHY-9017077.

Appendix A

In this Appendix, we review the derivation of the QRPA equation from the equation of motion method. In the equation of motion, the excited eigenstates $|m>$ are constructed from the phonon creation operator $Q_m^\dagger$ which is defined by

$$|m>= Q_m^\dagger|0>, \text{ and } Q_m|0>= 0, \text{ for all } m \tag{A.1}$$

where $|m>$ and $|0>$ are the excited eigenstate and the physical ground state. They satisfy the Schrödinger equations,

$$H|m>= E_m|m> \text{ and } H|0>= E_0|0> . \tag{A.2}$$

Then one obtains the following equation of motion from the above relations;

$$[H, Q_m^\dagger]|0>= (E_m - E_0)Q_m^\dagger|0> . \tag{A.3}$$

Multiplying from the left with an arbitrary state of the form $<0|\delta Q_m$, we get

$$<0|[\delta Q_m, [H, Q_m^\dagger]]|0>= \hbar\omega <0|[\delta Q_m, Q_m^\dagger]|0> \tag{A.4}$$

where $\hbar\omega = E_m - E_0$.

In order to derive the usual QRPA equation, we assume that the excited states are obtained by creating or destroying two quasiparticles from the QRPA ground state $|\text{QRPA}>$,

$$|m>= Q_m^\dagger|\text{QRPA}>= \sum_{k<k'}(X_{kk'}^m c_k^\dagger c_{k'}^\dagger - Y_{kk'}^m c_{k'} c_k)|\text{QRPA}> . \tag{A.5}$$

The QRPA ground state is defined by

$$Q_m|\text{QRPA}>= 0. \tag{A.6}$$

Inserting $Q_m^\dagger$ into the Eq. (A.4), and choosing δQ to be $c_{k'}c_k$ and $c_k^\dagger c_{k'}^\dagger$, one obtains the QRPA equation

$$\begin{pmatrix} A & B \\ -B^* & -A^* \end{pmatrix} \begin{pmatrix} X \\ Y \end{pmatrix} = \hbar\omega \begin{pmatrix} X \\ Y \end{pmatrix} . \tag{A.7}$$

The matrix elements are given by $(k < k', l < l')$

$$\begin{aligned} A_{kk',ll'} &= < \mathrm{QRPA}|[c_{k'}c_k, [H, c_l^\dagger c_{l'}^\dagger]]|\mathrm{QRPA} > \\ &\approx < \mathrm{BCS}|[c_{k'}c_k, [H, c_l^\dagger c_{l'}^\dagger]]|\mathrm{BCS} > \\ &= (E_k + E_{k'})\delta_{kl}\delta_{k'l'} + (H_{22})_{kk'll'} \end{aligned} \tag{A.8}$$

$$\begin{aligned} B_{kk',ll'} &= - < \mathrm{QRPA}|[c_{k'}c_k, [H, c_{l'}c_l]]|\mathrm{QRPA} > \\ &\approx - < \mathrm{BCS}|[c_{k'}c_k, [H, c_{l'}c_l]]|\mathrm{BCS} > \\ &= (H_{40})_{kk'll'} + (H_{40})_{ll'kk'} - (H_{40})_{klk'l'} - (H_{40})_{k'l'kl} \\ &\quad -(H_{40})_{l'kk'l} - (H_{40})_{lk'kl'} \end{aligned} \tag{A.9}$$

where we approximate the QRPA ground state as the BCS state in Eqs. (A.8-A.9).

Appendix B

In this Appendix, we will examine the relation between QRPA and pnQRPA equations. When we consider Eq. (A.5) including the proton and neutron components, it can be expanded as,

$$\begin{aligned} Q_m^\dagger &= \sum_{k<k'} (X_{kk'}^m c_k^\dagger c_{k'}^\dagger - Y_{kk'}^m c_{k'}c_k) \\ &= \sum_{p<p'} (X_{pp'}^{\mathrm{pp}} c_p^\dagger c_{p'}^\dagger - Y_{kk'}^{\mathrm{pp}} c_{p'}c_p) + \sum_{n<n'} (X_{nn'}^{\mathrm{nn}} c_n^\dagger c_{n'}^\dagger - Y_{kk'}^{\mathrm{nn}} c_{n'}c_n) \\ &\quad + \sum_{pn} (X_{pn}^{\mathrm{pn}} c_p^\dagger c_n^\dagger - Y_{kk'}^{\mathrm{pn}} c_n c_p). \end{aligned} \tag{B.1}$$

Inserting $Q_m^\dagger$ into the Eq. (A.4), and choosing the variational δQ to be $c_{p'}c_p$, $c_p^\dagger c_{p'}^\dagger$,

$c_{n'}c_n$, $c_n^\dagger c_{n'}^\dagger$, $c_n c_p$ and $c_p^\dagger c_n^\dagger$, one obtains,

$$\begin{pmatrix} A^{pp} & B^{pp} & C & D & & \\ -B^{pp*} & -A^{pp*} & -D^* & -C^* & & \\ F & D & A^{nn} & B^{nn} & & \\ -D^* & -F^* & -B^{nn*} & -A^{nn*} & & \\ & & & & A^{pn} & B^{pn} \\ & & & & -B^{pn*} & -A^{pn*} \end{pmatrix} \begin{pmatrix} X^{pp} \\ Y^{pp} \\ X^{nn} \\ Y^{nn} \\ X^{pn} \\ Y^{pn} \end{pmatrix} = \hbar\omega \begin{pmatrix} X^{pp} \\ Y^{pp} \\ X^{nn} \\ Y^{nn} \\ X^{pn} \\ Y^{pn} \end{pmatrix} . \tag{B.2}$$

The matrix elements A^{pp}, B^{pp}, A^{nn} and B^{nn} are given by Eqs. (A.8,A.9), and A^{pn}, and B^{pn} are given by Eqs. (11,12). The matrix elements C, D and F are expressed as

$$\begin{aligned} C_{pp',nn'} &= < \text{QRPA}|[c_{p'}c_p, [H, c_n^\dagger c_{n'}^\dagger]]|\text{QRPA} > \\ &\approx < \text{BCS}|[c_{p'}c_p, [H, c_n^\dagger c_{n'}^\dagger]]|\text{BCS} > \\ &= (P_{22}^{pn})_{pnp'n'} \end{aligned} \tag{B.3}$$

$$\begin{aligned} D_{pp',nn'} &= - < \text{QRPA}|[c_{p'}c_p, [H, c_{n'}c_n]]|\text{QRPA} > \\ &\approx - < \text{BCS}|[c_{p'}c_p, [H, c_{n'}c_n]]|\text{BCS} > \\ &= -(H_{40}^{pn})_{pnp'n'} - (H_{40}^{pn})_{p'n'pn} \\ &\quad +(H_{40})_{p'npn'} + (H_{40})_{pn'p'n} \end{aligned} \tag{B.4}$$

$$\begin{aligned} F_{pp',nn'} &= < \text{QRPA}|[c_{n'}c_n, [H, c_p^\dagger c_{p'}^\dagger]]|\text{QRPA} > \\ &\approx < \text{BCS}|[c_{n'}c_n, [H, c_p^\dagger c_{p'}^\dagger]]|\text{BCS} > \\ &= (N_{22}^{pn})_{pnp'n'}. \end{aligned} \tag{B.5}$$

From Eq. (B.2), we can find the sub-matrix in low-right corner is the pnQRPA equation which is decoupled from the proton-proton and neutron-neutron QRPA matrix located in up-left corner. The reason for the decoupling is that the operators associated with X^{pp}, Y^{pp} in Eq. (B.1) describe the states in the $(N, Z \pm 0, 2)$ nuclei;

and X^{nn}, Y^{nn} describe the $(N \pm 0, 2, Z)$ nuclei whereas and X^{pn}, Y^{pn} describe the $(N \pm 1, Z \pm 1)$ nuclei. Hence, the X^{pn}, Y^{pn} amplitudes decouple from the others. But X^{pp}, Y^{pp} and X^{nn}, Y^{nn} both can describe the (N, Z) nucleus and consequently couple together.

Appendix C

In this Appendix, we will introduce and discuss the coherent one-body transition density and coherent transition matrix element. In the second-quantization formalism, the one-body operator can be expressed by

$$F = \sum_{\alpha\beta} < \alpha|F|\beta > a^{\dagger}_{\alpha} a_{\beta}, \tag{C.1}$$

where $|\alpha >$ and $|\beta >$ are the single particle states. The transition matrix element between the initial state $|i >$ and the final state $|f >$ is given by

$$M_{fi} =< f|F|i >= \sum_{\alpha\beta} < \alpha|F|\beta >< f|a^{\dagger}_{\alpha} a_{\beta}|i > . \tag{C.2}$$

$< \alpha|F|\beta >$ is called the single-particle matrix element (SPME) which is only related to the single-particle states $|\alpha >$ and $|\beta >$. $< f|a^{\dagger}_{\alpha} a_{\beta}|i >$ is called the one-body transition density (OBTD), which is the function of the initial and final states as well as the single-particle states $|\alpha >$ and $|\beta >$. Then Eq. (C.2) can be rewritten as

$$M_{fi} = \sum_{o} \mathrm{SPME}(o)\mathrm{OBTD}(o, f, i), \tag{C.3}$$

where o represents the single-particle states.

Now we introduce a *coherent state* $|\mathrm{C} >$ which is defined by

$$|\mathrm{C} >= N_{\mathrm{C}} F|i > , \tag{C.4}$$

where N_{C} is the normalization factor which is determined by

$$< \mathrm{C}|\mathrm{C} > \; = \; N^2_{\mathrm{C}} < i|F^{\dagger}F|i >$$

$$= N_C^2 \sum_f < i|F^\dagger|f >< f|F|i > . \qquad \text{(C.5)}$$

Then we have

$$N_C = \frac{1}{\sqrt{\sum_f < f|F|i >^2}}. \qquad \text{(C.6)}$$

The transition matrix element between the coherent state and initial state is

$$\begin{aligned} < C|F|i > &= N_C < i|F^\dagger F|i > \\ &= N_C \sum_f < i|F^\dagger|f >< f|F|i > \\ &= N_C \sum_{o,f} M_{fi} \mathrm{SPME}(o)\mathrm{OBTD}(o,f,i) \\ &= \sum_o \mathrm{SPME}(o)\mathrm{COBTD}(o,i) \\ &= \sum_o \mathrm{CTME}(o,i). \end{aligned} \qquad \text{(C.7)}$$

where the COBTD and CTME are the *coherent one-body transition density* and *coherent transition matrix element* which are defined by

$$\begin{aligned} \mathrm{COBTD}(o,i) &= N_C \sum_f M_{fi} \mathrm{OBTD}(o,f,i) \\ \mathrm{CTME}(o,i) &= \mathrm{SPME}(o)\mathrm{COBTD}(o,f,i). \end{aligned} \qquad \text{(C.8)}$$

The COBTD and CTME are a function of the single-particle state and initial state. It represents the single-particle state effects in the total transition strength and depends only on the structure of the initial state.

References

[1] P.J. Brussaard and P.W.M. Glaudemans, *Shell Model Applications in Nuclear Spectroscopy* North-Holland, Amsterdam, 1977.

[2] M. Morita, *Beta Decay and Muon Capture*, Advanced Book Program, Reading, Massachusetts, 1973.

[3] W.C. Haxton and G.J. Stephenson, Prog. Part. Nucl. Phys. **12**, (1984), 409.

[4] M. Doi, T. Kotani and E. Takasugi, Prog. Theor. Phys. suppl. **83**, (1985), 1.

[5] K. Muto and H.V. Klapdor, in *Neutrinos* Editor, H.V. Klapdor (Springer-Verlag, 1988)

[6] J.D. Vergados, Phys. Rep. **133**, (1986), 1.

[7] S.R. Elliott, A.A. Hahn and M.K. Moe Phys. Rev. Lett., **59**, (1987), 2020.

[8] F.T. Avignone III, et. al, Phys. Lett. **256B**, (1991), 559.

[9] H. Ejiri, et. al., Phys. Lett. **258B**, (1991), 17.

[10] A.L. Turkevich, T.E. Economou and G.A. Cowan, Phys. Rev. lett., **67**, (1991), 3211.

[11] B.A. Brown and B.H. Wildenthal, Ann. Rev. of Nucl. Part. Sci. **38**, (1988), 29.

[12] J.A. Halbeib and R.A. Sorensen, Nucl. Phys. **A98**, (1967), 542.

[13] D. Cha, Phys. Rev.**C27**, (1983), 2269.

[14] A.H. Wapstra and N.B. Gove, Nucl. Data Table **9**, (1971), 265.

[15] Kleinheinz, et. al., Phys. Rev. Lett. **55**, (1985), 2664.

[16] J. Suhonen, A. Faessler, T. Taigel, and T. Tomoda, Phys. Lett. **202B**, (1988), 174; J. Suhonen, T. Taigel, and A. Faessler, Nucl. Phys. **A486**, (1988), 91.

[17] P. Vogel and M.R. Zirnbaur, Phys. Rev. Lett. **57** (1986), 3148.

[18] O. Civitarese, A. Faessler and T. Tomada, Phys. Lett. **194B**, (1987), 11.

[19] J. Engel, P. Vogel and M.R. Zirnbauer, Phys. Rev. **C37**, (1988), 731.

[20] K. Muto, E. Bender and H.V. Klapdor, Z. Phys. **A333**, (1989), 125; K. Muto, E. Bender and H.V. Klapdor, Z. Phys. **A334**, (1989), 177; K. Muto, E. Bender and H.V. Klapdor, Z. Phys. **A334**, (1989), 187.

[21] M. Hirsch, et.al., Nucl. Phys. **A535**, (1991), 62

[22] B. Lauritzen, Nucl. Phys. **A489**, (1988), 237.

[23] B.A. Brown and L. Zhao, *Nuclear weak Process and Nuclear Structure* , Edited by A. M. Morita, et. al. p291, Singapore: World Sci., (1989).

[24] O. Civitarese, H. Müther, L.D. Skouras and A. Faessler, J. Phys. G: Nucl. Part. Phys. **17**, (1991), 1363.

[25] N. Auerbach, G.F. Bertsch, B.A. Brown and L. Zhao, " β^+ Gamow-Teller strength in Nuclei ", preprint, submitted to Nucl. Phys. **A**.

[26] K. Muto, E. Bender and H.V. Klapdor, Z. Phys. **A339**, (1991), 435.

[27] D.J. Rowe, *Nuclear Collective Motion*, Methuen, London, (1970).

[28] P. Ring and P. Schuck, *The Nuclear Many-Body Problem* , Springer-Verlag, New York, (1980).

[29] A. Etchegoyen, W.D.M. Rae, N.S. Godwin, W.A. Richter, C.H. Zimmerman, B.A. Brwon, W.E. Ormand and J.S. Winfield, MSU-NSCL report #524 (1985).

[30] K. Grotz and H.V. Klapdor, Nucl. Phys. **A460**, (1986), 395.

[31] W.A. Richter, M.G.V.D. Merwe, R.E. Julies and B.A. Brown, Nucl. Phys. **A523**, (1991), 325.

[32] B.A. Brown and R. Sherr, Nucl. Phys. **A322**, (1979), 61.

[33] R.D. Lawson, *Theory of the Nuclear Shell Model*, Clarendon Press, Oxford, (1980).

[34] B.A. Brown and L. Zhao, *Understanding the Variety of Nuclear Excitations* , Edited by A. Covello, p497, Singapore: World Sci., (1990).

[35] Tsuboi, K. Muto, and H. Horie, Phys. Lett. **143B**, (1984), 293.

[36] L. Zhao, B.A. Brown, and W.A. Richter, Phys. Rev. **C42**, (1990), 1120.

Table 1: ^{46}Ti: Proton and neutron single particle energies ε_i (MeV), gap parameters Δ_i (MeV) and occupation probabilities v_i^2 from BCS and the shell-model E_i(SM) and v_i^2(SM) . The Fermi energies obtained from the BCS calculation are -12.968 MeV and -10.868 MeV for proton and neutron, respectively.

level	ε_i	Δ_i	v_i^2	E_i(BCS)	E_i(SM)	v_i^2(SM)
$\pi f_{7/2}$	-12.234	1.206	0.239	1.412	1.412	0.187
$\pi p_{3/2}$	-8.194	0.911	0.009	4.861	4.305	0.078
$\pi f_{5/2}$	-5.739	1.314	0.008	7.347	6.845	0.022
$\pi p_{1/2}$	-5.994	0.874	0.004	7.028	6.431	0.031
$\nu f_{7/2}$	-10.809	1.447	0.480	1.448	1.414	0.404
$\nu p_{3/2}$	-6.852	1.104	0.018	4.164	3.336	0.092
$\nu f_{5/2}$	-4.044	1.574	0.013	7.003	6.099	0.054
$\nu p_{1/2}$	-4.553	1.069	0.007	6.405	5.564	0.040

Table 2: ^{46}Ca: Neutron single particle energies ε_i (MeV), gap parameters Δ_i (MeV) and occupation probabilities v_i^2 and quasineutron energies E_i (MeV) from BCS, the shell-model E_i(SM), v_i^2(SM) (see text). The neutron Fermi energy is -8.712 MeV.

level	ε_i	Δ_i	v_i^2	E_i	E_i(SM)	v_i^2(SM)
$\nu f_{7/2}$	-9.395	1.347	0.726	1.510	1.700	0.703
$\nu p_{3/2}$	-5.507	1.042	0.025	3.370	3.343	0.049
$\nu f_{5/2}$	-3.354	1.455	0.013	5.552	6.377	0.025
$\nu p_{1/2}$	-3.107	1.026	0.008	5.698	5.830	0.016

Table 3: Comparison of the coherent transition matrix elements (CTME) obtained in the pnQRPA, "hybrid" pnQRPA and shell-model calculations of ^{46}Ti.

(A): CTME in the pnQRPA with BCS occupation and quasiparticle energies;
(B): CTME in the pnQRPA with BCS occupation and SM quasiparticle energies;
(C): CTME in the pnQRPA with SM occupation and BCS quasiparticle energies;
(D): CTME in the pnQRPA with SM occupation and quasiparticle energies;
(E): CTME in shell-model.

$j_p \rightarrow j_n$	A	B	C	D	E
$f_{7/2} \rightarrow f_{7/2}$	0.108	0.088	0.011	-0.070	-0.308
$f_{7/2} \rightarrow f_{5/2}$	1.641	1.706	1.187	1.223	1.431
$p_{3/2} \rightarrow p_{3/2}$	0.005	0.000	0.199	0.191	0.014
$p_{3/2} \rightarrow f_{5/2}$	0.000	0.000	0.000	0.000	0.000
$p_{3/2} \rightarrow p_{1/2}$	0.011	0.009	0.202	0.206	0.139
$f_{5/2} \rightarrow f_{7/2}$	-0.325	-0.391	-0.353	-0.433	-0.319
$f_{5/2} \rightarrow p_{3/2}$	0.000	0.000	0.000	0.000	0.000
$f_{5/2} \rightarrow f_{5/2}$	-0.002	-0.003	0.016	0.012	0.024
$p_{1/2} \rightarrow p_{3/2}$	-0.006	-0.010	0.028	0.015	-0.020
$p_{1/2} \rightarrow p_{1/2}$	0.000	0.000	0.010	0.011	0.002

Figure captions

Figure 1 Running sum of the Gamow-Teller strength $B(\mathrm{GT}^+, E_m)$ for ^{46}Ti $\rightarrow$^{46}Sc as a function of the ^{46}Sc 1^+ excitation energies relative to the ^{46}Ti ground state

Figure 2 Running sum of the Gamow-Teller strength $B(\mathrm{GT}^-, E_m)$ for ^{46}Ca $\rightarrow$^{46}Sc a function of the ^{46}Sc 1^+ excitation energies relative to the ^{46}Ca ground state

Figure 3 Running sum of the $2\nu\beta\beta$ decay matrix element $M_{\mathrm{GT}}(E_m)$ as a function of the ^{46}Sc 1^+ excitation energies relative to the ^{46}Ca ground state

Figure 4 Running sum of the closure $2\nu\beta\beta$ decay matrix element $B_{\mathrm{CLS}}(E_m)$ as a function of the ^{46}Sc 1^+ excitation energies relative to the ^{46}Ca ground state

Figure 5 Running sum of $B(\mathrm{GT}^+, E_m)$ for ^{46}Ti $\rightarrow$^{46}Sc in the pnQRPA with various g_{pp}, $(g_{ph} = 1)$

Figure 6 Running sum of $M_{\mathrm{GT}}(E_m)$ in the pnQRPA with various g_{pp}, $(g_{ph} = 1)$.

Figure 7 Running sum of $B_{\mathrm{CLS}}(E_m)$ in the pnQRPA with various g_{pp}, $(g_{ph} = 1)$.

Figure 8 Running sum of $B(\mathrm{GT}^+, E_m)$ in the pnQRPA, in which we project $B(\mathrm{GT}^+)$ onto the excitations constructed from ^{46}Ca β^- decay.

Figure 9 Running sum of the Gamow-Teller strength $B(\mathrm{GT}^+, E_m)$ in the "hybrid" pnQRPA.

Figure 10 Running sum of $B_{\mathrm{CLS}}(E_m)$ in the "hybrid" pnQRPA.

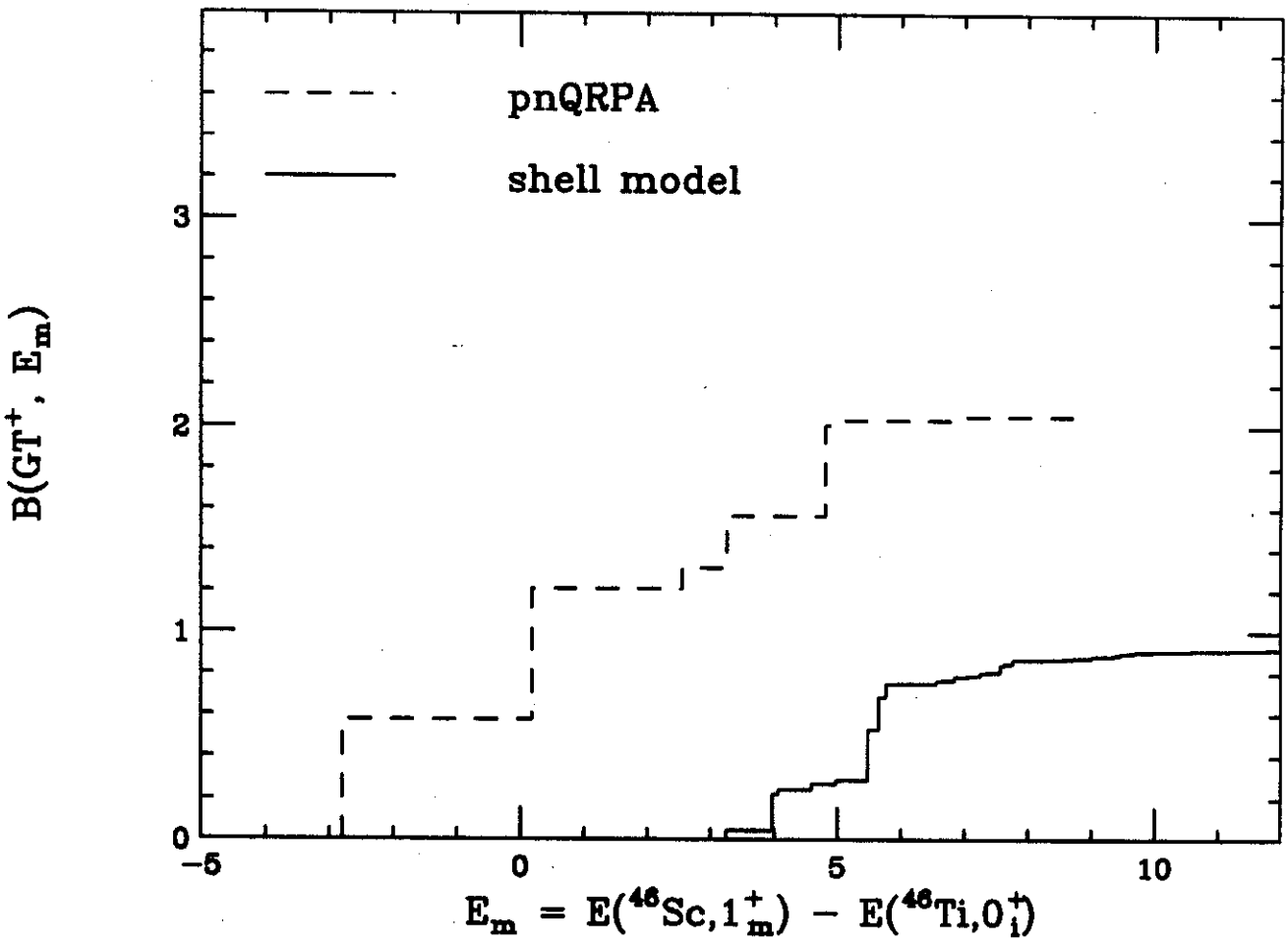

FIGURE 1

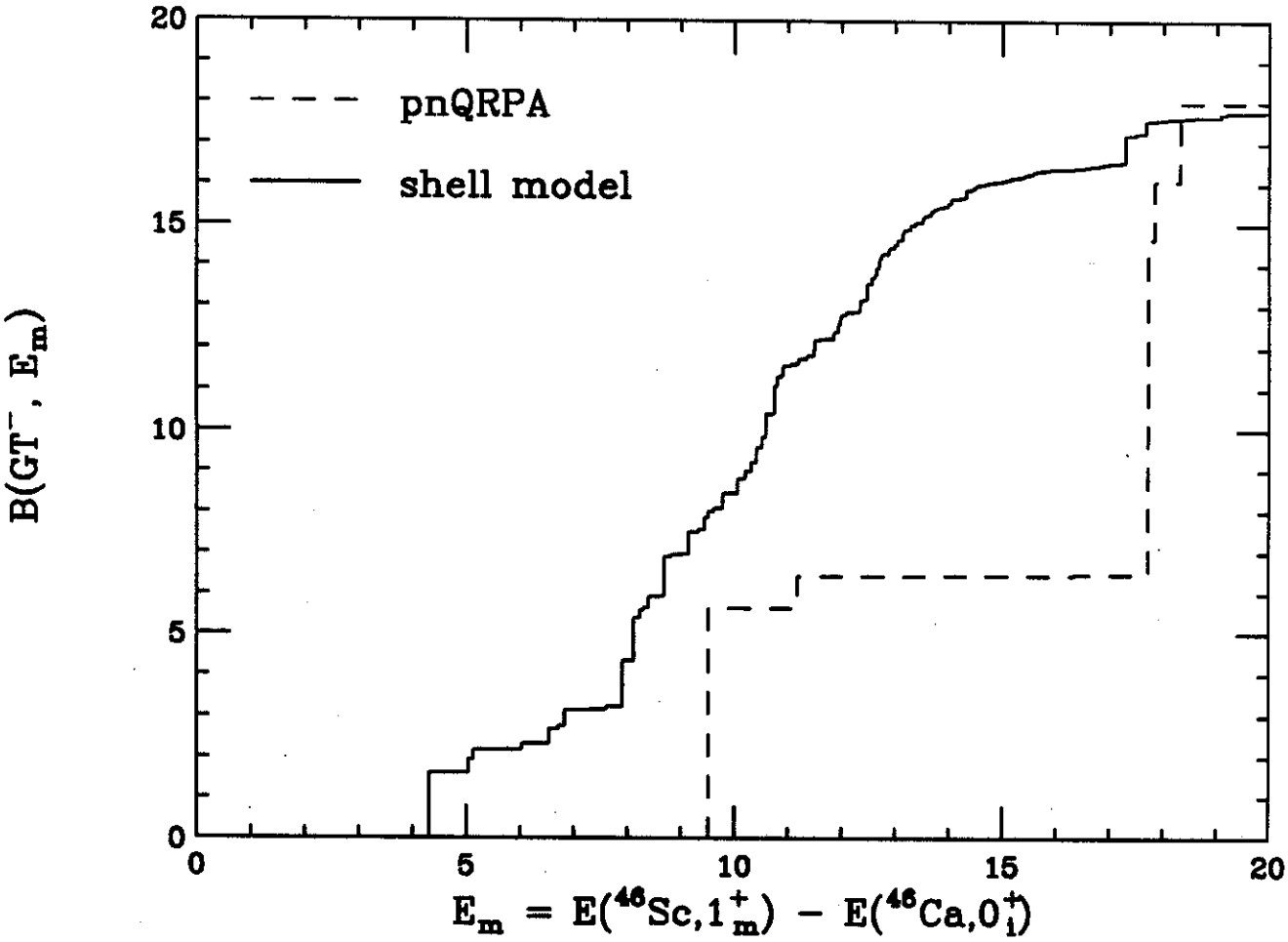

FIGURE 2

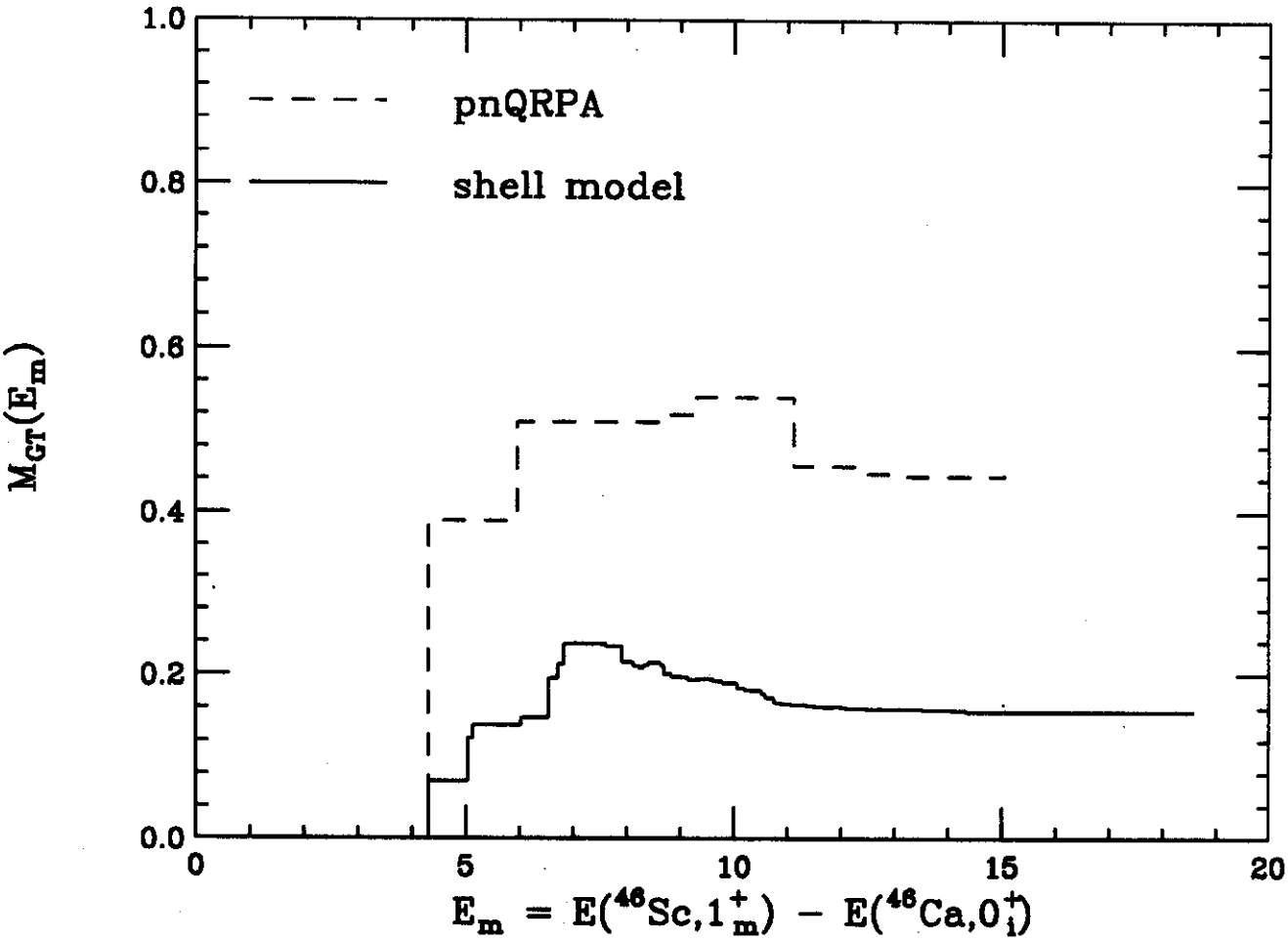
1.0
0.8
0.6
0.4
0.2
0.0
0
5
10
15
20
pnQRPA
shell model
$M_{GT}(E_m)$
$E_m = E(^{46}Sc,1^+_m) - E(^{46}Ca,0^+_i)$

FIGURE 3

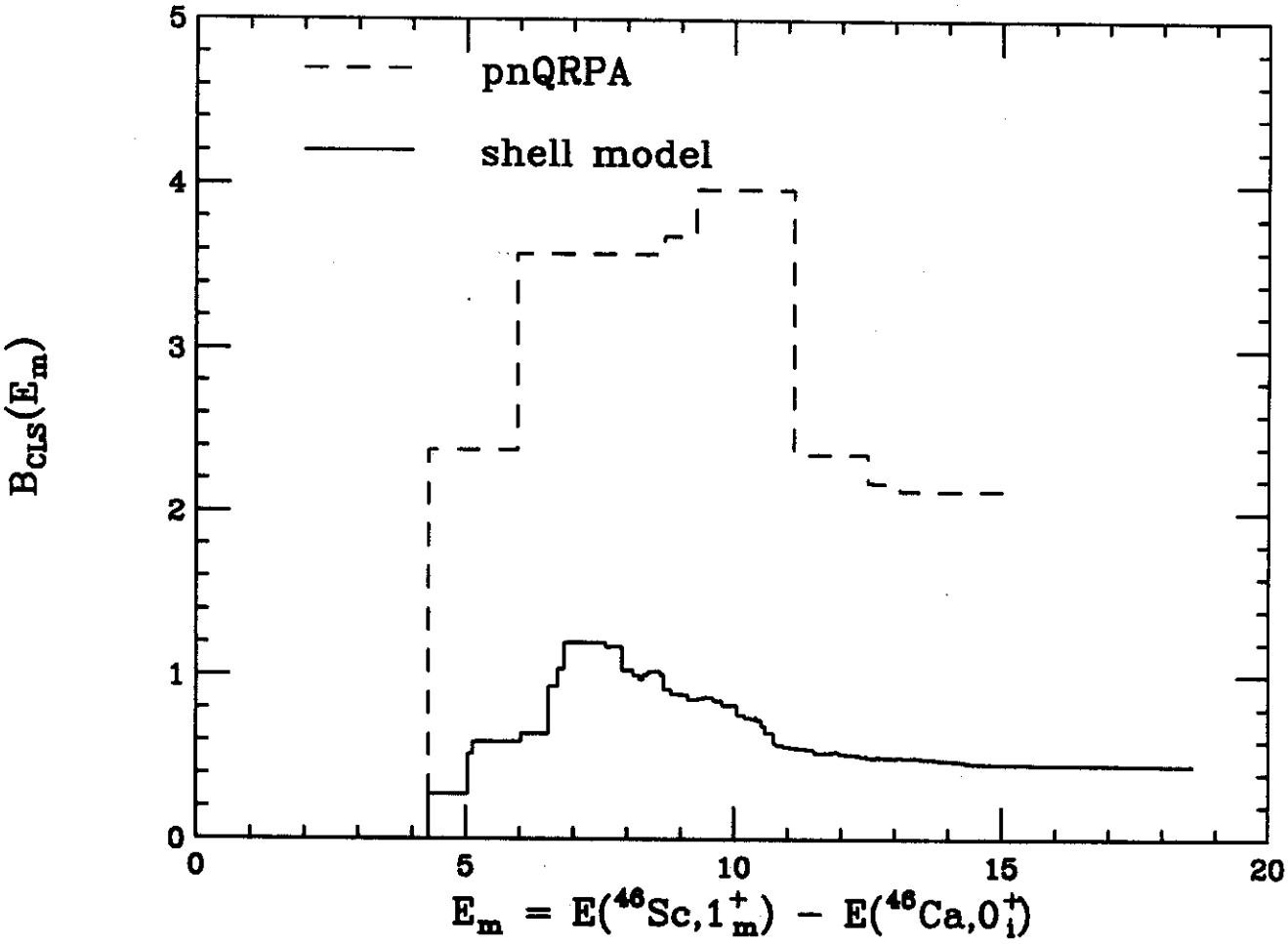
pnQRPA
shell model
$B_{CLS}(E_m)$
$E_m = E(^{46}Sc,1^+_m) - E(^{46}Ca,0^+_1)$
0
1
2
3
4
5
0
5
10
15
20

FIGURE 4

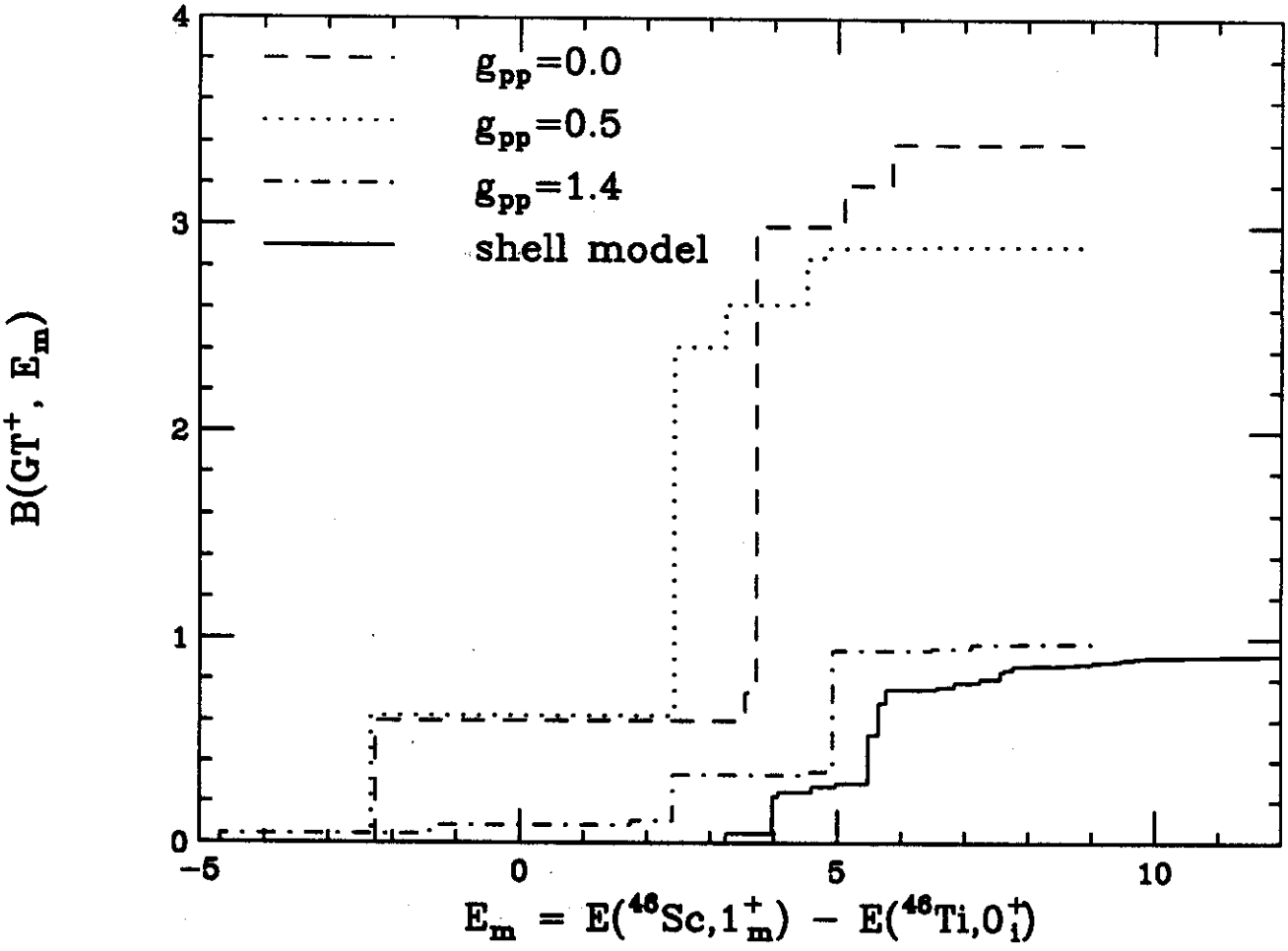
g_{pp}=0.0
g_{pp}=0.5
g_{pp}=1.4
shell model
B(GT$^+$, E_m)
E_m = E(^{46}Sc,1^+_m) − E(^{46}Ti,0^+_1)
0
1
2
3
4
−5
0
5
10

FIGURE 5

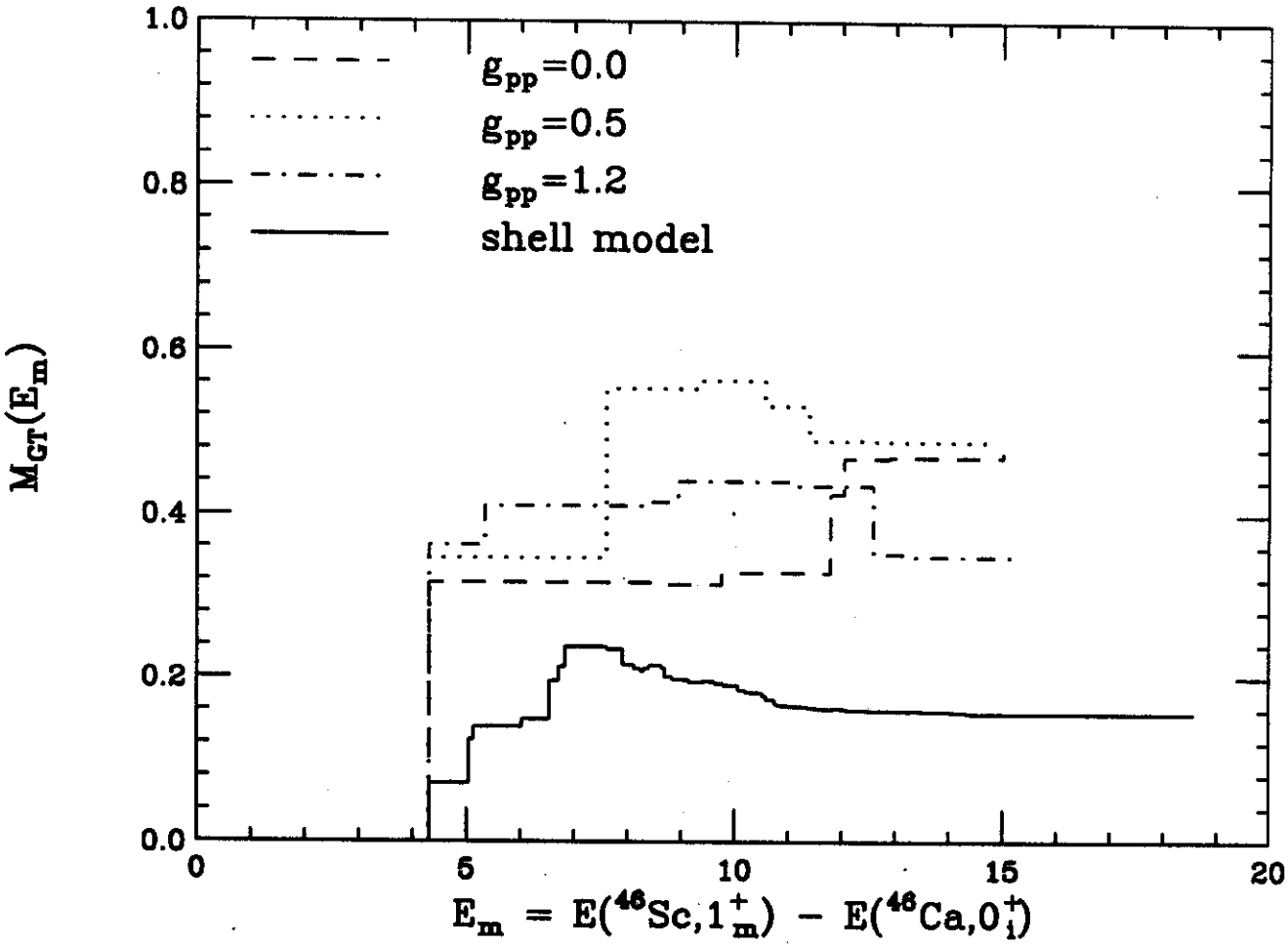
1.0
0.8
0.6
0.4
0.2
0.0
0
5
10
15
20
g_{pp}=0.0
g_{pp}=0.5
g_{pp}=1.2
shell model
$M_{GT}(E_m)$
$E_m = E(^{46}Sc,1^+_m) - E(^{46}Ca,0^+_i)$

FIGURE 6

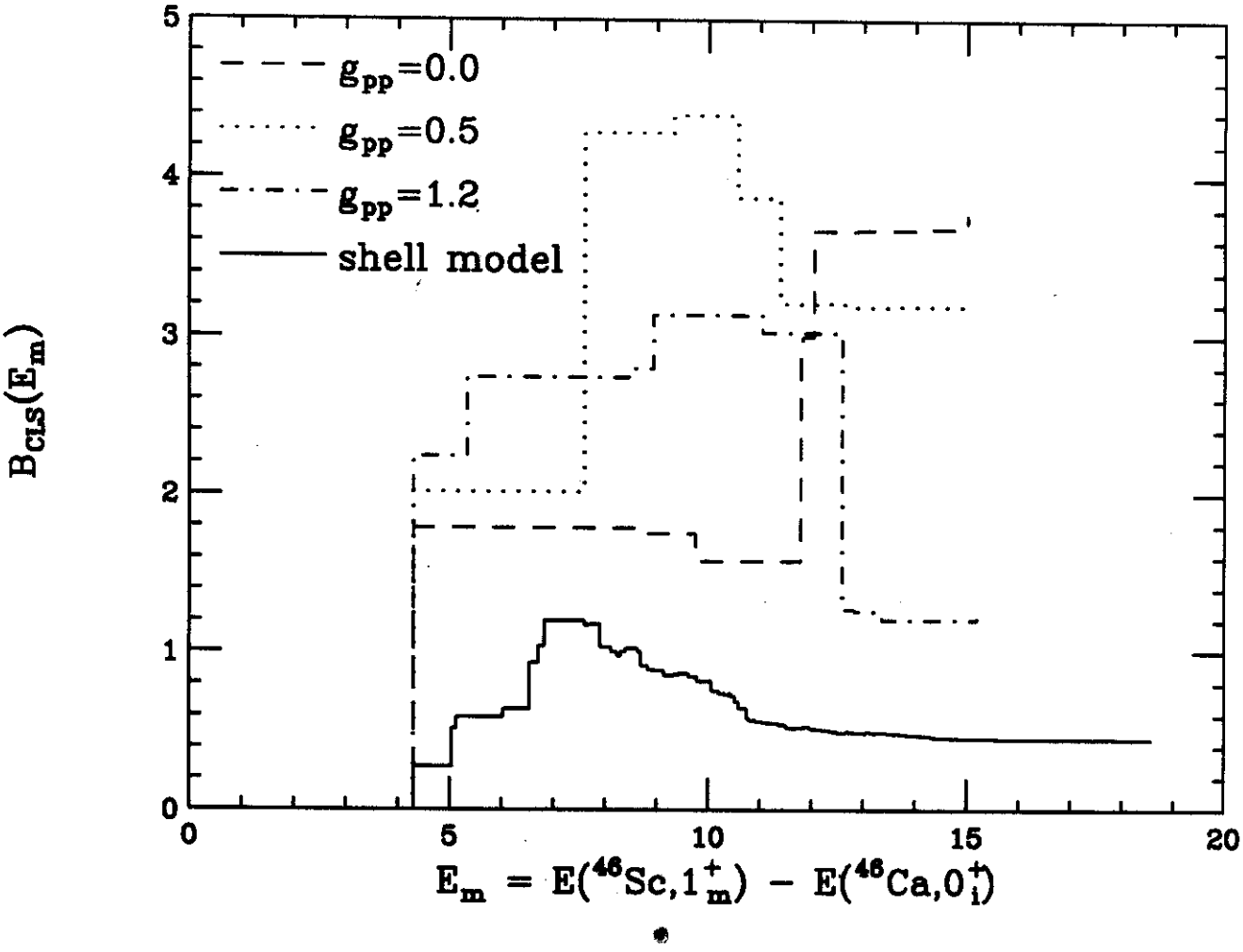
g_{pp}=0.0
g_{pp}=0.5
g_{pp}=1.2
shell model
$B_{CLS}(E_m)$
$E_m = E(^{46}Sc,1^+_m) - E(^{46}Ca,0^+_i)$
0
1
2
3
4
5
0
5
10
15
20

FIGURE 7

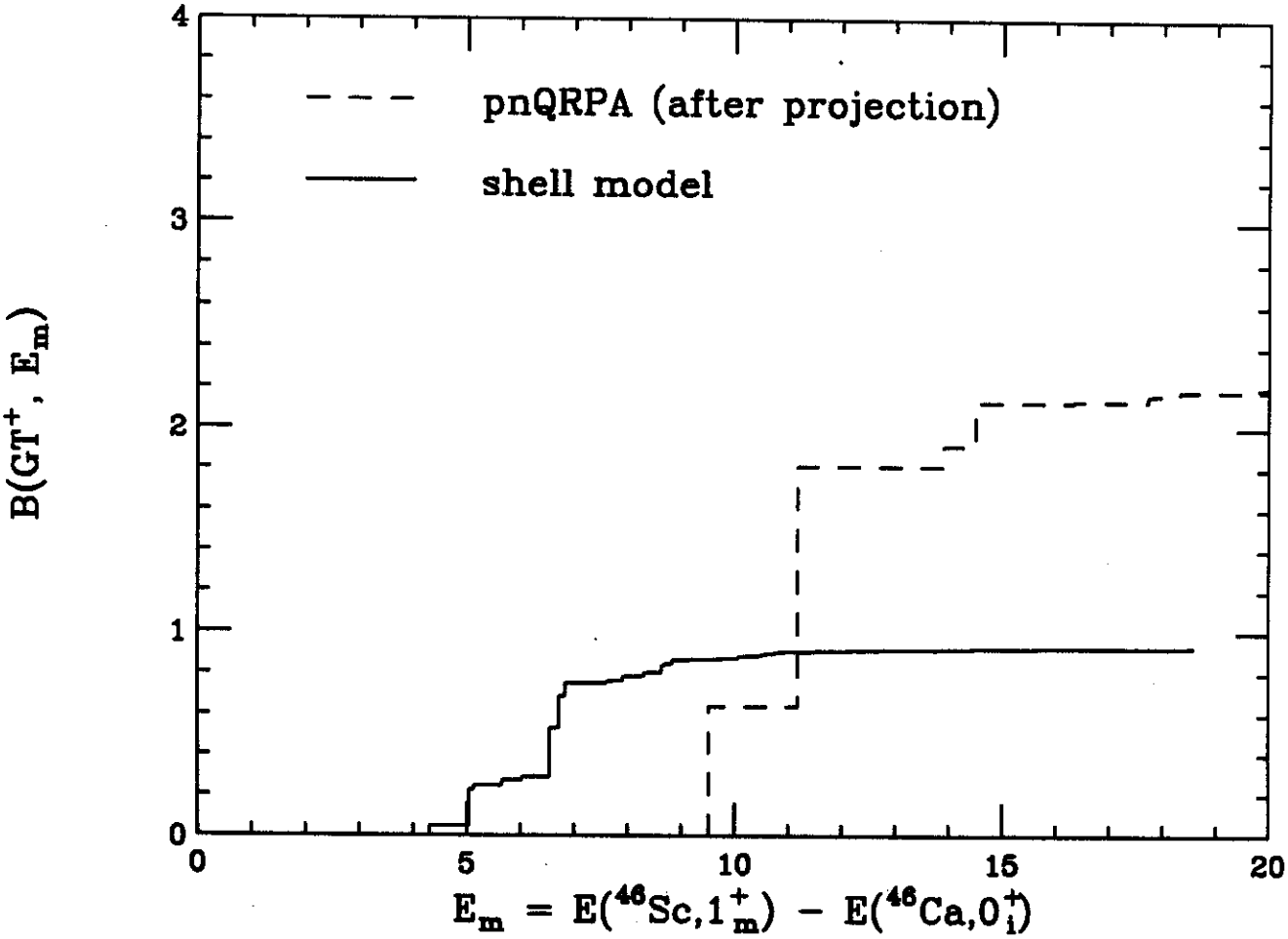
pnQRPA (after projection)
shell model
B(GT+, Em)
Em = E(46Sc,1+m) − E(46Ca,0+i)
0
1
2
3
4
0
5
10
15
20

FIGURE 8

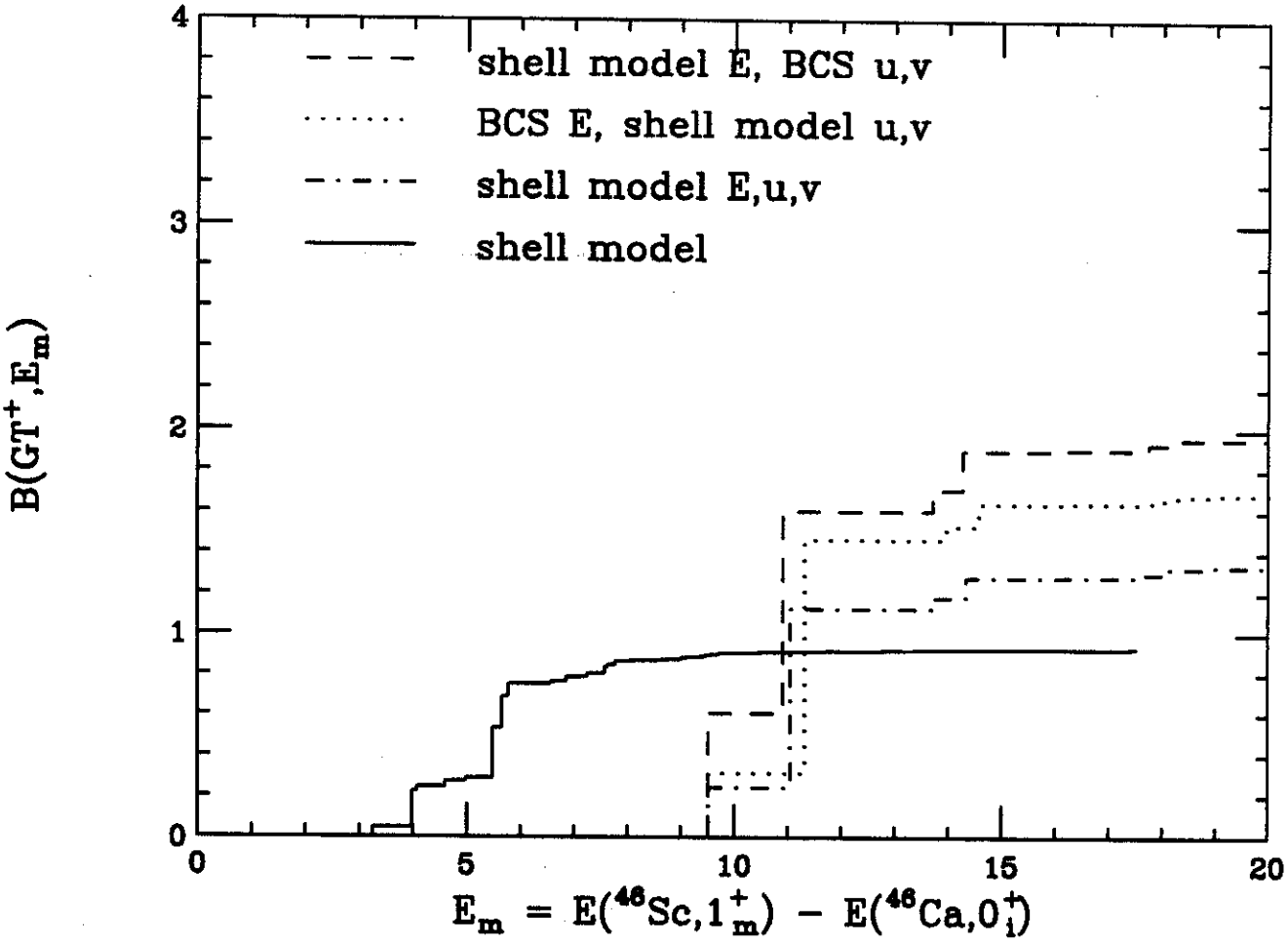
shell model E, BCS u,v
BCS E, shell model u,v
shell model E,u,v
shell model
B(GT+,Em)
Em = E(46Sc,1+m) − E(46Ca,0+i)
0
1
2
3
4
5
10
15
20

FIGURE 9

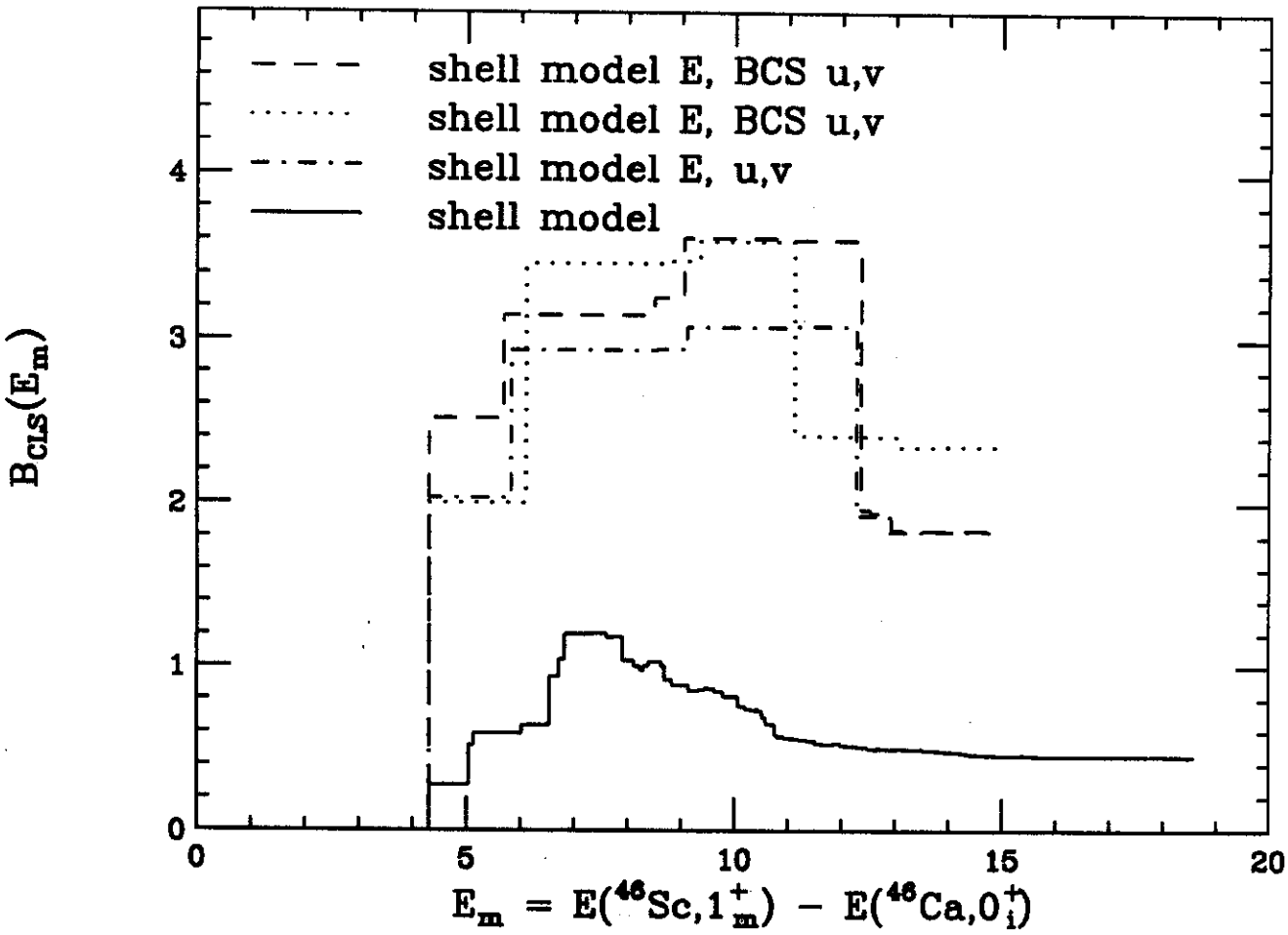
shell model E, BCS u,v
shell model E, BCS u,v
shell model E, u,v
shell model
$B_{CLS}(E_m)$
$E_m = E(^{46}Sc,1^+_m) - E(^{46}Ca,0^+_i)$
0
1
2
3
4
5
10
15
20

FIGURE 10